JOURNAL OF THERMOPHYSICS AND HEAT TRANSFER
Vol. 22, No. 3, July–September 2008

# Analytical Study of Heat Transfer from Elliptical Cylinder in Liquid Metals

R. Ahmad*
*COMSATS Institute of Information Technology, Abbottabad 22060, Pakistan*
and
W. A. Khan†
*National University of Sciences and Technology, PNS Jauhar, Karachi 75350, Pakistan*

DOI: 10.2514/1.36093

**Previous theoretical Nusselt numbers derived for the heat transfer to liquid metals flowing past an elliptical cylinder were based on the usual assumptions associated with inviscid potential flow. Although, in liquid metals, the thickness of the thermal boundary layer is much greater than the thickness of the hydrodynamic boundary layer, the effects of the thin hydrodynamic boundary layer on the heat transfer process cannot be neglected. In this study, the influence of a thin hydrodynamic boundary layer on the heat transfer from a single elliptical cylinder to liquid metals having low Prandtl numbers (0.001–0.03) is investigated under isothermal and isoflux boundary conditions. Two separate analytical heat transfer models, viscous and inviscid, are developed to clarify the discrepancy between previous results. It is demonstrated that the inviscid model gives higher heat transfer coefficients than the viscid model for both thermal boundary conditions, and the disagreement between the inviscid and viscous flow models originates due to the neglect of the hydrodynamic boundary layer compared to the thermal boundary layer and the effect of the separation of flow on heat transfer.**

## Nomenclature

| | | |
|---|---|---|
| $a$ | = | semimajor axis of elliptical cylinder, m |
| $b$ | = | semiminor axis of elliptical cylinder, m |
| $c_p$ | = | fluid specific heat, kJ/kg · K |
| $D$ | = | diameter of circular cylinder |
| $E(e)$ | = | complete elliptic integral of second kind |
| $e$ | = | eccentricity $\equiv \sqrt{1-\epsilon^2}$ |
| $h_{\text{av}}$ | = | average heat transfer coefficient, W/m$^2$ · K |
| $k$ | = | thermal conductivity, W/m · K |
| $\mathcal{L}$ | = | characteristic length $\equiv 4aE(e)/\pi$, m |
| $Nu_{\mathcal{L}}$ | = | Nusselt number based on the characteristic length $\equiv h\mathcal{L}/k_f$ |
| $Pe_{\mathcal{L}}$ | = | Peclet number based on characteristic length $\equiv Re_{\mathcal{L}}Pr$ |
| $Pr$ | = | Prandtl number $\equiv \nu/\alpha$ |
| $q$ | = | heat flux, W/m$^2$ |
| $Re_{\mathcal{L}}$ | = | Reynolds number based on characteristic length $\equiv U_{\text{app}}\mathcal{L}/\nu$ |
| $s$ | = | distance along curved surface of elliptical cylinder, m |
| $T$ | = | temperature, °C |
| $U_{\text{app}}$ | = | approach velocity, m/s |
| $U(s)$ | = | velocity in inviscid region just outside the boundary layer, m/s |
| $u$ | = | $s$ component of velocity in boundary layer, m/s |
| $v$ | = | $\eta$ component of velocity in boundary layer, m/s |
| $x, y$ | = | Cartesian coordinates |
| $\alpha$ | = | thermal diffusivity, m$^2$/s |
| $\delta$ | = | hydrodynamic boundary-layer thickness, m |
| $\delta_2$ | = | momentum boundary-layer thickness, m |
| $\delta_T$ | = | thermal boundary-layer thickness, m |
| $\epsilon$ | = | axis ratio $\equiv b/a$ |
| $\eta$ | = | distance normal to and measured from surface of an elliptical cylinder, m |
| $\theta$ | = | angle measured from stagnation point, radians |
| $\lambda$ | = | pressure gradient parameter |
| $\mu$ | = | absolute viscosity of fluid, kg/m · s |
| $\nu$ | = | kinematic viscosity of fluid, m$^2$/s |
| $\rho$ | = | fluid density, kg/m$^3$ |
| $\zeta$ | = | ratio of hydrodynamic to thermal boundary-layer thickness $\equiv \delta/\delta_T$ |
| $\tau$ | = | shear stress, N/m$^2$ |

*Subscripts*

| | | |
|---|---|---|
| $a$ | = | ambient |
| $f$ | = | fluid |
| $H$ | = | hydrodynamic |
| $p$ | = | pressure |
| $s$ | = | separation |
| $T$ | = | thermal |
| $w$ | = | wall |

## Introduction

THE use of liquid metals as a "thermal medium" in nuclear reactor and power-generating systems is increasing day by day due to their excellent heat transfer characteristics. An elliptical cylinder in liquid metals can be used more effectively in high-heat-flux applications. They offer less flow resistance and higher heat transfer rates than circular cylinders. They provide more general geometrical configurations than the circular cylinders. In the limiting cases, they represent a finite-length plate when the axis ratio $\epsilon \to 0$, and a circular cylinder when the axis ratio $\epsilon \to 1$. Thus, a systematic analytical investigation of elliptical geometries can provide not only flow and heat transfer characteristics from elliptical cylinders of different axis ratios but also from circular cylinders and finite-length flat plates. Khan et al. [1] reported several studies related to fluid flow and heat transfer from elliptic cylinders to Newtonian fluids having Prandtl numbers $\geq 0.7$. In an another paper, Khan et al. [2] presented other studies [3–10] related to heat transfer from cylinders to liquid metals ($0.001 \leq Pr \leq 0.03$). Theoretical studies [3–6] were based on potential flow and were used to determine the heat transfer coefficients of liquid metals for flow across flat plates and normal to

Received 7 December 2007; revision received 3 March 2008; accepted for publication 3 March 2008. 

*Research Associate, Department of Mathematics.
†Associate Professor, PN College of Engineering, Department of Engineering Sciences.

cylinders of various cross sections. They derived theoretical expressions for the average Nusselt numbers for different surface temperature profiles. In experimental/numerical studies [7–10], local and average heat transfer coefficients were determined for the flow of liquid sodium normal to a single circular cylinder. They found a considerable discrepancy between their experimental/numerical results and the previous analytical predictions, and concluded that the assumption of potential flow was inadequate to predict accurately the heat transfer rate.

The purpose of this study is to investigate the effects of a thin hydrodynamic boundary on the heat transfer from an elliptical cylinder. The potential and viscous flows are studied and analytical models are developed for local and average heat transfer coefficients using isothermal and isoflux thermal boundary conditions. The values of the axis ratio $\epsilon$ are taken from 0.1 to 1.

For a fair comparison of heat transfer from an elliptical cylinder with that of a circular cylinder, a characteristic length is used in both $Re_{\mathcal{L}}$ and $Nu_{\mathcal{L}}$. This characteristic length $\mathcal{L}$ is based on the equivalent diameter of a circular cylinder whose parameter is the same as that of the elliptical cylinder and that of the flat plate. The characteristic length $\mathcal{L} = 4aE(e)/\pi$ where $E(e)$ is the complete elliptical integral. In the limiting cases, when $\epsilon \to 1$, this characteristic length gives the diameter $D$ of a circular cylinder, and when $\epsilon \to 0$, it represents the length $L$ of a flat plate.

## Analysis

Consider a uniform flow of a liquid metal with low Prandtl number past a fixed elliptic cylinder of the characteristic length $\mathcal{L}$. The approaching velocity of the fluid is $U_{\text{app}}$ and the ambient temperature is assumed to be $T_a$. The surface temperature of the elliptic cylindrical wall is $T_w$, where $T_w \geq T_a$ in the case of the isothermal cylinder and the heat flux is $q$ for the isoflux boundary conditions. The flow is assumed to be laminar, steady, and two-dimensional. An integral approach is employed for the boundary-layer analysis to derive closed-form expressions for the calculation of local and average heat transfer coefficients. The von Kármán–Pohlhausen method [11,12] is used to solve the momentum equation and the energy equation is solved for both thermal boundary conditions. A fourth-order velocity profile in the hydrodynamic boundary layer and a third-order temperature profile in the thermal boundary layer are used. Khan et al. [1] set up the momentum and energy equations in a curvilinear system of coordinates in which $s$ denotes the distance along the curved surface of the elliptic cylinder measured from the forward stagnation point $A$, and $\eta$ is the distance normal to and measured from the surface. In this system of coordinates, the velocity components are denoted by $u$ and $v$ in the local $s$ and $\eta$ directions. For the viscous flow model, the velocity distribution in the thin hydrodynamic boundary layer can be approximated by a fourth-order polynomial as suggested by Pohlhausen [12]:

$$\frac{u}{U(s)} = \left[(2\eta_H - 2\eta_H^3 + \eta_H^4) + \frac{\lambda}{6}(\eta_H - 3\eta_H^2 + 3\eta_H^3 - \eta_H^4)\right] \quad (1)$$

where $\eta_H = \eta/\delta$ is the dimensionless distance normal to the cylinder surface in the hydrodynamic boundary layer, and $U(s)$ is the potential flow velocity over an elliptical cylinder just outside the boundary layer and can be written as

$$U(s) = \frac{(1+\epsilon)U_{\text{app}} \sin\theta}{\sqrt{1 - e^2\cos^2\theta}} \quad (2)$$

Khan et al. [1] solved the momentum equation using the von Kármán–Pohlhausen integral method [11,12] and obtained the following expressions for the dimensionless boundary-layer and momentum thicknesses:

$$\left.\begin{aligned} \frac{\delta}{\mathcal{L}} &= \frac{1}{2\sqrt{Re_{\mathcal{L}}}} \sqrt{\frac{\pi\lambda(1-e^2\cos^2\theta)^2}{\epsilon^2(1+\epsilon)E(e)\cos\theta}} \\ \frac{\delta_2}{\mathcal{L}} &= \frac{0.61}{\sqrt{Re_{\mathcal{L}}}} \sqrt{\frac{(1-e^2\cos^2\theta)^3}{E(e)\sin^6\theta} \int_0^\theta \frac{\sin^5\theta \mathrm{d}\theta}{(1-e^2\cos^2\theta)^2}} \end{aligned}\right\} \quad (3)$$

The energy equation in the curvilinear system is

$$u\frac{\partial T}{\partial s} + v\frac{\partial T}{\partial \eta} = \alpha\frac{\partial^2 T}{\partial \eta^2} \quad (4)$$

The thermal boundary conditions for the isothermal and isoflux cylinders are as follows:

$$\eta = 0; \qquad \begin{cases} T = T_w & \text{UWT} \\ \frac{\partial T}{\partial \eta} = -\frac{q}{k_f} & \text{UWF} \end{cases} \quad (5)$$

and

$$\eta = \delta_T; \qquad \begin{cases} T = T_a & \text{UWT} \\ \frac{\partial T}{\partial \eta} = 0 & \text{UWF} \end{cases} \quad (6)$$

where UWT and UWF are the uniform wall temperature and uniform wall flux, respectively. Temperature distributions for both thermal boundary conditions will be

$$T - T_a = \begin{cases} (T_w - T_a)\left(1 - \frac{3}{2}\eta_T + \frac{1}{2}\eta_T^3\right) & \text{UWT} \\ \frac{2q\delta_T}{3k_f}\left(1 - \frac{3}{2}\eta_T + \frac{1}{2}\eta_T^3\right) & \text{UWF} \end{cases} \quad (7)$$

## Inviscid Model

In liquid metals, the thickness of the viscous boundary layer is small as compared with that of the thermal boundary layer and may be ignored, so that the fluid flow can be considered as a potential flow of an ideal fluid. Assuming the presence of a thin thermal boundary layer $\delta_T$ along the cylinder surface, the energy integral equation can be written as

$$\frac{\mathrm{d}}{\mathrm{d}s}\int_0^{\delta_T}(T - T_a)u\,\mathrm{d}\eta = \begin{cases} -\alpha\frac{\partial T}{\partial \eta}\Big|_{\eta=0} & \text{UWT} \\ \frac{q}{\rho c_p} & \text{UWF} \end{cases} \quad (8)$$

Using temperature profiles, Eq. (7), and assuming $\zeta = \delta/\delta_T \ll 1$, Eq. (8) can be simplified to

$$\left.\begin{aligned} \delta_T\tfrac{\mathrm{d}}{\mathrm{d}s}[U(s)\delta_T] &= 4\alpha \quad \text{UWT} \\ \tfrac{\mathrm{d}}{\mathrm{d}s}[U(s)\delta_T^2] &= \tfrac{4\nu}{Pr} \quad \text{UWF} \end{aligned}\right\} \quad (9)$$

In the case of elliptical geometry, the radial distance $r$ to a point on the ellipse surface is

$$r = a\sqrt{1 - e^2\cos^2\theta} \quad (10)$$

therefore, the length $ds$ can be written as

$$ds = a\sqrt{1 - e^2\cos^2\theta}\,d\theta \quad (11)$$

Solving Eqs. (9), the dimensionless thermal boundary-layer thickness for both boundary conditions can be written as

$$\frac{\delta_T(\theta)}{\mathcal{L}} \cdot \sqrt{Pe_{\mathcal{L}}} = \begin{cases} \sqrt{\frac{2\pi(1-e^2\cos^2\theta)}{E(e)(1+\epsilon)(1+\cos\theta)}} & \text{UWT} \\ \sqrt{\frac{\pi(1-e^2\cos^2\theta)^{1/2}f(\theta)}{E(e)(1+\epsilon)\sin\theta}} & \text{UWF} \end{cases} \quad (12)$$

where

$$f(\theta) = \int_0^\theta \sqrt{1 - e^2\cos^2\theta}\,\mathrm{d}\theta \quad (13)$$

Using a basic definition, heat transfer coefficients for both thermal boundary conditions can be written as

$$h(\theta) = 1.5\frac{k_f}{\mathcal{L}}\sqrt{Pe_{\mathcal{L}}}\begin{cases}\sqrt{\frac{E(e)(1+\epsilon)(1+\cos\theta)}{2\pi(1-e^2\cos^2\theta)}} & \text{UWT}\\ \sqrt{\frac{E(e)(1+\epsilon)\sin\theta}{\pi(1-e^2\cos^2\theta)^{1/2}f(\theta)}} & \text{UWF}\end{cases} \tag{14}$$

In dimensionless form, these heat transfer coefficients can be written as

$$\frac{Nu_{\mathcal{L}}(\theta)}{\sqrt{Pe_{\mathcal{L}}}} = 1.5\begin{cases}\sqrt{\frac{E(e)(1+\epsilon)(1+\cos\theta)}{2\pi(1-e^2\cos^2\theta)}} & \text{UWT}\\ \sqrt{\frac{E(e)(1+\epsilon)\sin\theta}{\pi(1-e^2\cos^2\theta)^{1/2}f(\theta)}} & \text{UWF}\end{cases} \tag{15}$$

The average heat transfer coefficient, for both thermal boundary conditions, can be defined as

$$h = \frac{1}{\pi}\int_0^{\pi} h(\theta)\,\mathrm{d}\theta$$

In dimensionless form, it can be written as

$$\frac{Nu_{\mathcal{L}}}{\sqrt{Pe_{\mathcal{L}}}} = \frac{1.5}{\pi}\begin{cases}\int_0^{\pi}\sqrt{\frac{E(e)(1+\epsilon)(1+\cos\theta)}{2\pi(1-e^2\cos^2\theta)}}\,\mathrm{d}\theta & \text{UWT}\\ \int_0^{\pi}\sqrt{\frac{E(e)(1+\epsilon)\sin\theta}{\pi(1-e^2\cos^2\theta)^{1/2}f(\theta)}}\,\mathrm{d}\theta & \text{UWF}\end{cases} \tag{16}$$

Equation (16) is solved for different values of $\epsilon$ and the results are correlated in terms of $\epsilon$ into single correlation for each thermal boundary condition.

$$\frac{Nu_{\mathcal{L}}}{\sqrt{Pe_{\mathcal{L}}}} = \begin{cases}\frac{1.66+7.14\epsilon}{1+9.28\epsilon-1.07\epsilon^2} & \text{UWT}\\ \frac{2.25+10.5\epsilon}{1+10.91\epsilon-0.17\epsilon^2} & \text{UWF}\end{cases} \tag{17}$$

The results of inviscid models for both thermal boundary conditions are presented and compared with Hsu [5] analytical models in Table 1 for the same axis ratios.

## Viscous Flow Model

In this model, the velocity distribution, Eq. (1), is used inside the hydrodynamic boundary layer, whereas the potential flow velocity, Eq. (2), is used outside the boundary layer. The thermal boundary conditions, Eqs. (5) and (6), and the temperature distributions, Eq. (7), for isothermal and isoflux cylinders are the same for this model. Following the procedure used by Khan et al. [1] and neglecting higher powers of $\zeta$, Eq. (8) for both thermal boundary conditions can be simplified to

$$\left.\begin{aligned}\delta_T\cdot\tfrac{\mathrm{d}}{\mathrm{d}s}\left[U(s)\delta_T\left(\tfrac{3}{8}-\tfrac{3\zeta}{10}+\tfrac{\zeta\lambda}{120}\right)\right] &= \tfrac{3\alpha}{2} \quad \text{UWT}\\ \tfrac{\mathrm{d}}{\mathrm{d}s}\left[\delta_T^2U(s)\left(\tfrac{3}{8}-\tfrac{3\zeta}{10}+\tfrac{\zeta\lambda}{120}\right)\right] &= \tfrac{3\nu}{2Pr} \quad \text{UWF}\end{aligned}\right\} \tag{18}$$

**Table 1 Dimensionless heat transfer values for inviscid model under isothermal and isoflux boundary conditions**

| Axis ratio $\epsilon$ | Present model $Nu_{\mathcal{L}}/\sqrt{Pe_{\mathcal{L}}}$ | | Hsu [5] $Nu_{\mathcal{L}}/\sqrt{Pe_{\mathcal{L}}}$ | |
|---|---|---|---|---|
| | UWT | UWF | UWT | UWF |
| 0.1 | 1.235 | 1.579 | 1.164 | 1.313 |
| 0.2 | 1.096 | 1.371 | 1.176 | 1.326 |
| 0.3 | 1.029 | 1.271 | 1.173 | 1.323 |
| 0.4 | 0.995 | 1.210 | 1.160 | 1.308 |
| 0.5 | 0.975 | 1.169 | 1.141 | 1.286 |
| 0.6 | 0.964 | 1.141 | 1.118 | 1.261 |
| 0.7 | 0.959 | 1.120 | 1.093 | 1.232 |
| 0.8 | 0.955 | 1.105 | 1.067 | 1.203 |
| 0.9 | 0.953 | 1.094 | 1.041 | 1.174 |
| 1.0 | 0.952 | 1.086 | 1.015 | 1.145 |

where $\zeta = \delta/\delta_T \ll 1$ and $\lambda$ is the pressure gradient parameter whose values were determined by Khan et al. [1] by solving the momentum integral equation for different values of axis ratio $\epsilon$. These values were found to be positive from $0 \le \theta \le \theta_1 = 90$ deg (region 1, bounded by ACOA) and negative from $\theta_1 \le \theta \le \theta_s$ (region 2, bounded by CODC), as shown in Fig. 1. Thus, the entire range of interest $0 \le \theta \le \theta_s$ could be divided into two regions and the $\lambda$ values were fitted separately by the least-square method into two polynomials for each axis ratio $\epsilon$. Neglecting higher powers of $\zeta$ and depending upon values of $\lambda$, Eq. (18), for the isothermal boundary condition, can be written for the two regions

$$\left.\begin{aligned}\delta_{T_1}^2\left[\tfrac{9}{64}-\tfrac{3\zeta}{4}\left(\tfrac{\lambda}{120}-\tfrac{3}{10}\right)\right] &= \tfrac{3a\alpha}{U_{\text{app}}(1+\epsilon)}\cdot\tfrac{1-e^2\cos^2\theta}{\sin^2\theta}f_1(\theta) \quad \text{region 1}\\ \left|\delta_T^2\left[\tfrac{9}{64}-\tfrac{3\zeta}{4}\left(\tfrac{\lambda}{120}-\tfrac{3}{10}\right)\right]\right|_{\delta_{T_1}}^{\delta_{T_2}} &= \tfrac{3a\alpha}{U_{\text{app}}(1+\epsilon)}\cdot\tfrac{1-e^2\cos^2\theta}{\sin^2\theta}f_2(\theta) \quad \text{region 2}\end{aligned}\right\} \tag{19}$$

where

$$\left.\begin{aligned}f_1(\theta) &= \int_0^{\theta}\sin\theta\left(\tfrac{3}{8}-\tfrac{3\zeta}{10}+\tfrac{\zeta\lambda_1}{120}\right)\mathrm{d}\theta \quad \text{region 1}\\ f_2(\theta) &= \int_{\pi/2}^{\theta}\sin\theta\left(\tfrac{3}{8}-\tfrac{3\zeta}{10}+\tfrac{\zeta\lambda_2}{120}\right)\mathrm{d}\theta \quad \text{region 2}\end{aligned}\right\} \tag{20}$$

Solving Eqs. (19) for dimensionless thermal boundary-layer thicknesses $\Delta_1 = \delta_{T_1}\sqrt{Pe_{\mathcal{L}}}/\mathcal{L}$ and $\Delta_2 = \delta_{T_2}\sqrt{Pe_{\mathcal{L}}}/\mathcal{L}$, we get a quadratic equation for each region:

$$\left.\begin{aligned}\Delta_1^2-\left(\tfrac{36-\lambda_1}{45}\right)\sqrt{\tfrac{\pi(1-e^2\cos^2\theta)^2\lambda_1 Pr}{\epsilon^2(1+\epsilon)E(e)\cos\theta}}\Delta_1-\tfrac{2\pi(1-e^2\cos^2\theta)Pr}{E(e)(1+\epsilon)(1+\cos\theta)} &= 0 \quad \text{region 1}\\ \Delta_2^2-\left(\tfrac{36-\lambda_2}{45}\right)\sqrt{\tfrac{\pi(1-e^2\cos^2\theta)^2\lambda_2 Pr}{\epsilon^2(1+\epsilon)E(e)\cos\theta}}\Delta_2-\tfrac{16\pi(1-e^2\cos^2\theta)f_3(\theta)}{3E(e)(1+\epsilon)\sin^2\theta} &= 0 \quad \text{region 2}\end{aligned}\right\} \tag{21}$$

where $f_3(\theta) = f_1(\theta) + f_2(\theta)$. The solution of Eqs. (21) gives the dimensionless thermal boundary-layer thickness in both regions.

$$\begin{aligned}\Delta_1 &= \frac{36-\lambda_1}{90}\sqrt{\frac{\lambda_1 Pr\pi(1-e^2\cos^2\theta)^2}{\epsilon^2(1+\epsilon)E(e)\cos\theta}}\\ &\quad+\frac{1}{90}\sqrt{\frac{(36-\lambda_1)^2\lambda_1 Pr\pi(1-e^2\cos^2\theta)^2}{\epsilon^2(1+\epsilon)E(e)\cos\theta}+\frac{16200\pi(1-e^2\cos^2\theta)}{E(e)(1+\epsilon)(1+\cos\theta)}}\\ &= F_1(\theta,\epsilon,Pr)\end{aligned} \tag{22}$$

and

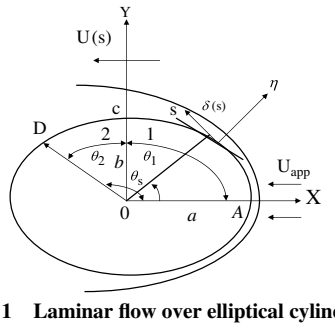


**Fig. 1 Laminar flow over elliptical cylinder.**

$$\Delta_2 = \frac{36-\lambda_2}{90}\sqrt{\frac{\lambda_2 Pr\pi(1-e^2\cos^2\theta)^2}{\cos\theta\epsilon^2(1+\epsilon)E(e)}} + \frac{1}{90}\sqrt{\frac{(36-\lambda_2)^2\lambda_2 Pr\pi(1-e^2\cos^2\theta)^2}{\cos\theta\epsilon^2(1+\epsilon)E(e)} + \frac{16200\pi(1-e^2\cos^2\theta)(1-2\cos\theta)}{E(e)(1+\epsilon)\sin^2\theta}} = F_2(\theta,\epsilon,Pr) \quad (23)$$

The local heat transfer coefficient in both regions can be written as

$$\left.\begin{aligned} h_1(\theta) &= \frac{3k_f}{2\Delta_{T_1}} = \frac{3k_f}{2\mathcal{L}}\frac{\sqrt{Pe_\mathcal{L}}}{F_1(\theta,\epsilon,Pr)} \quad \text{region 1} \\ h_2(\theta) &= \frac{3k_f}{2\Delta_{T_1}} = \frac{3k_f}{2\mathcal{L}}\frac{\sqrt{Pe_\mathcal{L}}}{F_1(\theta,\epsilon,Pr)} \quad \text{region 2} \end{aligned}\right\} \quad (24)$$

Thus, the local Nusselt numbers for UWT, in both regions, will be

$$\left.\begin{aligned} \frac{Nu_{\mathcal{L}_1}(\theta)}{\sqrt{Pe_\mathcal{L}}} &= \frac{1.5}{F_1(\theta,\epsilon,Pr)} \quad \text{region 1} \\ \frac{Nu_{\mathcal{L}_2}(\theta)}{\sqrt{Pe_\mathcal{L}}} &= \frac{1.5}{F_2(\theta,\epsilon,Pr)} \quad \text{region 2} \end{aligned}\right\} \quad (25)$$

Following the same procedure for the uniform wall flux boundary condition, Eq. (18) can be written for two regions and solved for dimensionless thermal boundary-layer thicknesses $\Delta_1$ and $\Delta_2$. The corresponding solutions for UWF can be written as

$$\Delta_1 = \frac{36-\lambda_1}{180}\sqrt{\frac{\lambda_1 Pr\pi(1-e^2\cos^2\theta)^2}{\epsilon^2(1+\epsilon)E(e)\cos\theta}} + \frac{1}{180}\sqrt{\frac{(36-\lambda_1)^2\lambda_1 Pr\pi(1-e^2\cos^2\theta)^2}{\epsilon^2(1+\epsilon)E(e)\cos\theta} + \frac{32400\pi f(\theta)\sqrt{1-e^2\cos^2\theta}}{E(e)(1+\epsilon)\sin\theta}} = G_1(\theta,\epsilon,Pr) \quad (26)$$

and

$$\Delta_2 = \frac{36-\lambda_2}{180}\sqrt{\frac{\lambda_2 Pr\pi(1-e^2\cos^2\theta)^2}{\epsilon^2(1+\epsilon)E(e)\cos\theta}} + \frac{1}{180}\sqrt{\frac{(36-\lambda_2)^2\lambda_2 Pr\pi(1-e^2\cos^2\theta)^2}{\epsilon^2(1+\epsilon)E(e)\cos\theta} + \frac{32400\pi f_5(\theta)\sqrt{1-e^2\cos^2\theta}}{E(e)(1+\epsilon)\sin\theta}} = G_2(\theta,\epsilon,Pr) \quad (27)$$

where $f(\theta)$ can be determined from Eq. (13), $f_5(\theta) = f(\theta) + f_4(\theta)$, and

$$f_4(\theta) = \int_{\pi/2}^{\theta}\sqrt{1-e^2\cos^2\theta}\,\mathrm{d}\theta \quad (28)$$

Using the definition of the heat transfer coefficient and Eq. (24), local Nusselt numbers for UWF in both regions can be written as

$$\left.\begin{aligned} \frac{Nu_{\mathcal{L}_1}(\theta)}{\sqrt{Pe_\mathcal{L}}} &= \frac{1.5}{G_1(\theta,\epsilon,Pr)} \quad \text{region 1} \\ \frac{Nu_{\mathcal{L}_2}(\theta)}{\sqrt{Pe_\mathcal{L}}} &= \frac{1.5}{G_2(\theta,\epsilon,Pr)} \quad \text{region 2} \end{aligned}\right\} \quad (29)$$

Thus, the local Nusselt numbers from the front stagnation point to the separation point, for both thermal boundary conditions, can be written as

$$\frac{Nu_\mathcal{L}(\theta)}{\sqrt{Pe_\mathcal{L}}} = 1.5\begin{cases} \frac{1}{F_1(\theta,\epsilon,Pr)} + \frac{1}{F_2(\theta,\epsilon,Pr)} & \text{UWT} \\ \frac{1}{G_1(\theta,\epsilon,Pr)} + \frac{1}{G_2(\theta,\epsilon,Pr)} & \text{UWF} \end{cases} \quad (30)$$

The average heat transfer coefficient can be defined as

$$h_{\mathrm{av}} = \frac{1}{\pi}\int_0^\pi h(\theta)\,\mathrm{d}\theta = \frac{1}{\pi}\left[\int_0^{\pi/2} h(\theta)\,\mathrm{d}\theta + \int_{\pi/2}^{\theta_s} h(\theta)\,\mathrm{d}\theta + \int_{\theta_s}^{\pi} h(\theta)\,\mathrm{d}\theta\right]$$

The integral analysis is unable to predict heat transfer values from separation point to the rear stagnation point (third integral). However, experiments (Žukauskas and Žiugžda [13], Fand and Keswani [14], and Nakamura and Igarashi [15], among others) show that the heat transfer from the rear portion of the circular cylinder increases with Reynolds numbers. From a collection of all known data, Van der Hegge Zijnen [16] demonstrated that the heat transferred from the rear portion of the circular cylinder can be determined from $Nu_\mathcal{L} = 0.001Re_\mathcal{L}$ that does not depend upon the Prandtl number. However, no such information exists for the heat transfer from elliptical cylinders to liquid metals. Thus, the average heat transfer coefficient, in dimensionless form, from front stagnation point to the separation point for both thermal boundary conditions, can be written as

$$\frac{Nu_\mathcal{L}}{\sqrt{Pe_\mathcal{L}}} = \frac{1.5}{\pi}\begin{cases} \int_0^{\pi/2}\frac{\mathrm{d}\theta}{F_1(\theta,\epsilon,Pr)} + \int_{\pi/2}^{\theta_s}\frac{\mathrm{d}\theta}{F_2(\theta,\epsilon,Pr)} & \text{UWT} \\ \int_0^{\pi/2}\frac{\mathrm{d}\theta}{F_1(\theta,\epsilon,Pr)} + \int_{\pi/2}^{\theta_s}\frac{\mathrm{d}\theta}{F_2(\theta,\epsilon,Pr)} & \text{UWF} \end{cases} \quad (31)$$

The integrals in Eq. (31) are evaluated for different Prandtl numbers (0.001–0.03) and for axis ratios (0.1–1) and the results are fitted, for each thermal boundary condition, to a correlation in terms of Prandtl number and axis ratio. These correlations are given by

$$\frac{Nu_\mathcal{L}}{\sqrt{Re_\mathcal{L}}} = \begin{cases} \frac{(0.92+2.78\epsilon)Pr^{0.446(\epsilon+0.085)^{0.024}}}{1+6.75\epsilon-0.85\epsilon^2} & \text{UWT} \\ \frac{(8304+61410\epsilon)Pr^{(0.46+0.009\epsilon+0.016\epsilon^2-0.011\epsilon^3)}}{1+103632\epsilon+738\epsilon^2} & \text{UWF} \end{cases} \quad (32)$$

## Results and Discussion

Inviscid and viscous models for local and average heat transfer are developed for the flow of liquid metals across an elliptical cylinder under both isothermal and isoflux thermal boundary conditions. Local and average Nusselt numbers are calculated and compared with available results for both inviscid and viscous models using two liquid metals, liquid bismuth ($Pr = 0.0142$) and liquid sodium ($Pr = 0.0058$).

Figure 2 shows the comparison of local Nusselt numbers for the inviscid isothermal model. These local Nusselt numbers are compared with the Hsu [5] model for different axis ratios. It shows that the liquid bismuth with higher Prandtl number has higher Nusselt numbers. The local Nusselt numbers decrease quickly in the front and rear stagnation regions, whereas they decrease steadily in the middle region of the cylinder for both liquid metals. The

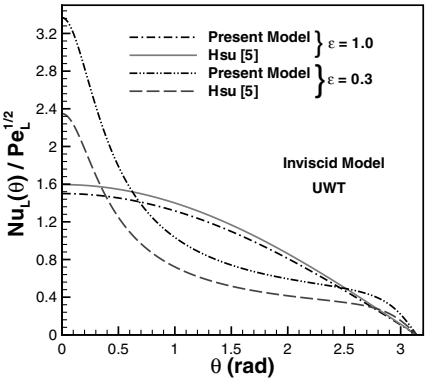


**Fig. 2 Comparison of local Nusselt numbers for inviscid isothermal model.**

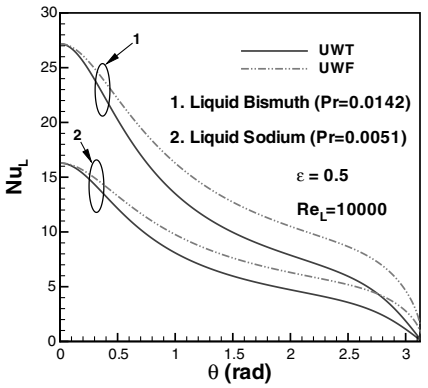


**Fig. 3 Comparison of inviscid models for isothermal and isoflux thermal boundary conditions.**

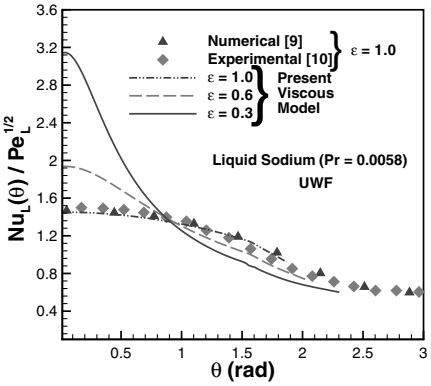


**Fig. 4 Comparison of local Nusselt numbers for viscous isoflux model.**

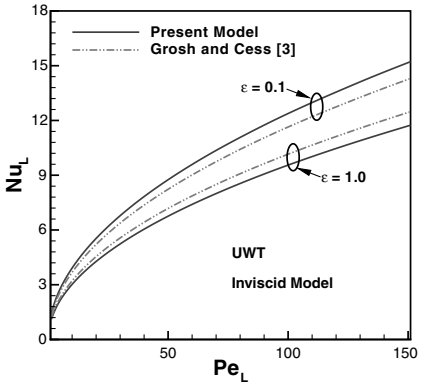


**Fig. 5 Comparison of average Nusselt numbers for inviscid isothermal model.**

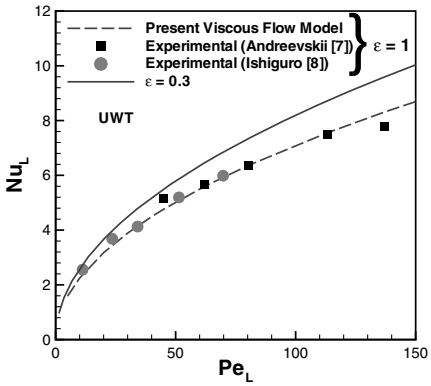


**Fig. 6 Average Nusselt numbers for viscous model under UWT.**

difference between the two models increases with the geometry from circular cylinder to flat plate. The local Nusselt numbers for both liquid metals are compared for isothermal and isoflux boundary conditions in Fig. 3. At the front and rear stagnation points, local Nusselt numbers are the same for both thermal boundary conditions and differ considerably at other points. As expected, the UWF boundary condition gives higher heat transfer coefficients than UWT. In Fig. 4, local Nusselt numbers of the viscous flow model are compared with experimental and numerical results using the UWF boundary condition. For $\epsilon = 1$, present results are in good agreement with the available experimental and numerical results. Again, the local Nusselt numbers decrease quickly in the front and rear stagnation regions and decrease steadily elsewhere when $\epsilon < 1$. It is observed that the viscous flow model yields lower local Nusselt numbers than the inviscid flow model for the same thermal boundary conditions. This is due to neglecting the hydrodynamic boundary layer compared with the thermal boundary layer and the effect of the separation of flow in the inviscid flow models.

Average Nusselt numbers of the present inviscid model are compared with Grosh and Cess [3] for UWT in Fig. 5. The results are compared for different axis ratios. It is observed that the average Nusselt numbers increase with the increase in Peclet numbers and decrease in axis ratio. This is mainly due to the increase in surface area. Thus, in the limiting cases, the heat transfer values are higher for a finite-length plate when the axis ratio $\epsilon \to 0$, and lower for a circular cylinder when the axis ratio $\epsilon \to 1$. The average Nusselt numbers of the viscous model are compared with available experimental results [7,8] for UWT (Fig. 6). The present results are in good agreement with the experimental results for $\epsilon = 1$. It is clear that the heat transfer values increase with the increase in eccentricity of an elliptical cylinder. The same behavior was observed for the UWF condition.

## Summary and Conclusions

Two separate viscous and inviscid flow models are developed for local and average heat transfer from a single elliptical cylinder to liquid metals for both isothermal and isoflux thermal boundary conditions. It is demonstrated that the disagreement between the inviscid and viscous flow models originates with the neglect of the hydrodynamic boundary layer compared with the thermal boundary layer and the effect of the separation of flow on heat transfer. The inviscid flow model gives higher local and average heat transfer coefficients than the viscous flow model. As expected, the heat transfer coefficients for both thermal boundary conditions increase with the decrease in axis ratio of the cylinder and the increase in Prandtl number.

## References

[1] Khan, W. A., Culham, J. R., and Yovanovich, M. M., "Fluid Flow Around and Heat Transfer from Elliptical Cylinders: Analytical Approach," *Journal of Thermophysics and Heat Transfer*, Vol. 19, No. 2, April–June 2005, pp. 178–185. doi:10.2514/1.10456

[2] Khan, W. A., Culham, J. R., and Yovanovich, M. M., "Analytical Study of Heat Transfer from Circular Cylinder in Liquid Metals," *Heat and Mass Transfer*, Vol. 42, No. 11, 2006, pp. 1017–1023. doi:10.1007/s00231-005-0068-4

[3] Grosh, R. J., and Cess, R. D., "Heat Transfer to Fluids with Low Prandtl Numbers for the Flow Across Plates and Cylinders of Various Cross Sections," *ASME Transactions. Journal of Tribology*, Vol. 80, No. 3, 1958, pp. 667–676.

[4] Grosh, R. J., and Cess, R. D., "Heat Transmission to Fluids with Low Prandtl Numbers for Flow Section Through Tube Banks," *ASME Transactions. Journal of Tribology*, Vol. 80, No. 3, 1958, pp. 677–682.

[5] Hsu, C. J., "Heat Transfer to Liquid Metals Flowing Past Spheres and Elliptical-Rod Bundles," *International Journal of Heat and Mass Transfer*, Vol. 8, No. 2, 1965, pp. 303–315. doi:10.1016/0017-9310(65)90118-3

[6] Hsu, C. J., "Analytical Study of Heat Transfer to Liquid Metals in Cross-Flow Through Rod Bundles," *International Journal of Heat and Mass Transfer*, Vol. 7, No. 43, 1964, pp. 431–436.

[7] Andreevskii, A. A., "Heat Transfer in Transverse Flow of Molten Sodium Around a Single Cylinder," *Soviet Journal of Atomic Energy*, Vol. 7, No. 3, 1961, pp. 745–747. doi:10.1007/BF01479967

[8] Ishiguro, R. K. T., Sugiyama, K., and Ikezaki, E., "Experimental Study of Heat Transfer Around a Circular Cylinder in a Liquid Sodium Cross Flow," *International Chemical Engineering*, Vol. 16, No. 2, 1976, pp. 249–253.

[9] Sugiyama, K., and Ishiguro, R., "Numerical Study of Local Heat Transfer Around a Circular Cylinder in a Liquid-Sodium Crossflow," *Heat Transfer*, Vol. 22, No. 7, 1978, pp. 59–68.

[10] Ishiguro, R., and Sugiyama, K. T., "Heat Transfer Across a Circular Cylinder in a Liquid Sodium Cross Flow," *International Journal of Heat and Mass Transfer*, Vol. 22, No. 7, 1979, pp. 1041–1048. doi:10.1016/0017-9310(79)90177-7

[11] Von Kármán, T., "Über Laminar Und Turbulente Reibung," *Zeitschrift für angewandte Mathematik und Mechanik*, Vol. 1, 1921, pp. 233–252.

[12] Pohlhausen, K., "Zur Näherungsweise Integration der Differential Gleichung der Laminaren Reibungschicht," *Zeitschrift für angewandte Mathematik und Mechanik*, Vol. 1, 1921, pp. 252–268.

[13] Žukauskas, A., and Žiugžda, J., *Heat Transfer of a Cylinder in Crossflow*, Hemisphere, New York, 1985.

[14] Fand, R. M., and Keswani, K. K., "Continuous Correlation Equation for Heat Transfer from Cylinders to Air in Crossflow for Reynolds Numbers from $10^{-2}$ to $2 \times 10^5$," *International Journal of Heat and Mass Transfer*, Vol. 15, No. 3, 1972, pp. 559–562. doi:10.1016/0017-9310(72)90219-0

[15] Nakamura, H., and Igarashi, T., "Variation of Nusselt Number with Flow Regimes Behind a Circular Cylinder for Reynolds Numbers from 70–30000," *International Journal of Heat and Mass Transfer*, Vol. 47, No. 23, 2004, pp. 5169–5173. doi:10.1016/j.ijheatmasstransfer.2004.05.034

[16] Van der Hegge Zijnen, B. G., "Modified Correlation Formulae for Heat Transfer by Natural and Forced Convection from Horizontal Cylinders," *Applied Scientific Research, Section A*, Vol. 6, Nos. 2–3, 1956, pp. 129–140.